JOURNAL OF SOLID STATE CHEMISTRY 107, 218–228 (1993)

The Structure of $Sr_2(VO_4)Cl$ and $Sr_2(CrO_4)Cl$ and Spectroscopic Properties of Mn^{5+}- and Cr^{5+}-Doped $Sr_2(VO_4)Cl$

C. ALBRECHT,* S. COHEN,† I. MAYER,† AND D. REINEN†,‡

*Fachbereich Chemie and Zentrum für Materialwissenschaften, Philipps-Universität Marburg, Germany; and †Department of Inorganic and Analytical Chemistry, Hebrew University, Jerusalem, Israel

Received December 22, 1992; accepted March 2, 1993

The structures of the spodiosite-type compounds $Sr_2(M^VO_4)Cl$ [M = V, Cr] and the spectroscopic properties (EPR, ligand field) of Mn^{5+}- and Cr^{5+}-doped $Sr_2(VO_4)Cl$ [$^3A_2$ and ^2E ground states in T_d, respectively] are reported. Evidence is presented that Cr^{5+} undergoes vibronic coupling effects of the Jahn–Teller type. Paramagnetic probe cations will only reflect the geometry of a host site, if they possess nondegenerate ground states in the respective symmetry and if their ionic radii are comparable to those of the host cations. © 1993 Academic Press, Inc.

Introduction

Transition metal ions with d^1 and d^2 configuration, such as Cr^{5+} and Mn^{5+} can be incorporated in the tetrahedral sites of compounds with the apatite [$A_5^{II}(M^VO_4)_3X$, with A^{II} = Ca, Sr, Ba; M^V = P, V; X^- = Cl^-, OH^-, F^-, etc.] and with the spodiosite structure [$A_2^{II}(M^VO_4)Cl$, with A^{II} = Ca, M^V = P, V, As and A^{II} = Sr, M^V = V, As]. The optical and EPR properties of Cr^{5+}-doped $Ca_2(PO_4)Cl$ single crystals were studied in great detail 20 years ago (*1*, *2*). These investigations have been extended to various other chloride spodiosite compounds recently, and in particular the angular dependence of the g-values of Cr^{5+} in Sr_2VO_4Cl has been measured (*3*). It has been suggested that the doped CrO_4^{3-} polyhedra do not adopt the geometry of the MO_4 polyhedra in the host compounds A_2MO_4Cl strictly. The Jahn–Teller instability of the ^2E ground state—though it is only π-antibonding—may induce a small additional distortion component, which would explain some contradictory results (*3*). We want to follow this argument further here, and will report in this connection the structures of Sr_2VO_4Cl and Sr_2CrO_4Cl, in order to complete the available structural informations about spodiosite-type compounds.

Mn^{5+}-doped spodiosites have also been studied by optical (*4*, *5*) and EPR spectroscopy (*5*). These compounds exhibit—as corresponding apatites—interesting luminescence properties (sharp-line $^1E \rightarrow {}^3A_2$ emissions) (*6*). The $^3A_2$ ground state is vibronically stable, and it is to be expected that Mn^{5+} adopts the respective MO_4 host geometry, if the size difference with respect to the M^V cation is small. While for Cr^{5+} the orientation of the g-tensor provides information about the polyhedron geometry, it is the fine-structure tensor in the case of Mn^{5+}, which is determined by the chemical bonding and the geometry of the MnO_4^{3-} polyhedron in the $A_2^{II}MO_4Cl$ host structure. We report here about the single-crystal EPR results on Mn^{5+}-doped Sr_2VO_4Cl, in comparison to the published results for Cr^{5+} in this compound (*3*).

In order to correlate the CrO_4^{3-} polyhe-

‡ To whom correspondence should be addressed.

0022-4596/93 $5.00

dron geometries with the d–d transition energies and the values and the orientations of the g-tensor components, we used the computer program CAMMAG (*7*). This program is based on describing the chemical bonding in the tetrahedron on the basis of the "angular-overlap-model" (AOM) (*8*). The corresponding static bonding picture has to be modified, however, because significant dynamic contributions due to $E \otimes \varepsilon$ vibronic coupling (E, electronic ground state symmetry in T_d; ε, Jahn–Teller active vibrational modes, inducing D_{2d} and D_2 distortions) are involved.

Experimental

The preparation of the compounds has been described elsewhere (*3*, *5*). We have observed that the preparation of single crystals of chloride apatites from ACl_2 melts [$A = Ca^{2+}$, Sr^{2+}, Ba^{2+}] reveals interesting thermodynamic properties of the apatite compared to the spodiosite compounds. The synthesis of apatite-type single crystals $A^{II}(MO_4)_3Cl$ [$M = P^V$, As^V, V^V, Cr^V] is only possible for $A = Ba^{2+}$ and with $A = Sr^{2+}$ in combination with P^V. In all the other cases crystals with the spodiosite structure and the constitution $A_2(MO_4)Cl$ are obtained. Apparently the spodiosite structure is thermodynamically more stable than the apatite lattice. It should be added, however, that one succeeds to prepare apatites of these constitutions as powders, if an excess of ACl_2 is avoided.

The EPR measurements between 298 and 4 K were performed with a Varian E 15 spectrometer at X- and Q-band frequencies. DPPH has been used as the internal standard.

Single crystals of Sr_2VO_4Cl and Sr_2CrO_4Cl with the approximate dimensions $0.13 \times 0.16 \times 0.20$ mm^3 and $0.13 \times 0.16 \times 0.24$ mm^3, respectively, were selected for the structure determination. They were mounted on a PW 1100/20 Philips four-cycle computer-controlled diffractometer, using Mo$K\alpha$ radiation ($\lambda = 0.71069$ Å) and a graphite monochromator. The scan range for each reflection was 1.0° with a constant scanning time of 10 sec. Background measurements were performed at each side of the scan for 10 sec. 682 and 659 unique reflection data up to $2\theta = 55°$ were collected in the case of the V^{5+} and Cr^{5+} spodiosite, respectively, and corrected for Lorentz and polarization effects. An absorption correction was performed only for Sr_2CrO_4Cl, because the temperature factors turned out to be rather large in this case; 526 and 514 reflections with structure factors larger than $6\sigma(F)$ for Sr_2VO_4Cl and Sr_2CrO_4Cl, respectively, were used for the refinement. The lattice parameters were determined on the basis of 24 reflections in the range $10° \leq \theta \leq 15°$. Both compounds crystallize in the spodiosite lattice with the orthorhombic space group Pbcm. The structure was refined with anisotropic temperature factors. The final reliability factors $R = \sum \| |F_o| - |F_c| \| / \sum |F_o|$ and $R_w = \{\sum w|F_o^2 - F_c^2|^2 / \sum wF_o^2\}^{1/2}$ were 0.045 and 0.063, respectively, for Sr_2VO_4Cl and 0.047 and 0.065 for Sr_2CrO_4Cl. The unit cell dimensions (Å) are:

	Sr_2CrO_4Cl	Sr_2VO_4Cl
a	6.475(2)	6.570(2)
b	7.426(2)	7.520(2)
c	11.359(3)	11.527(2)

The positional parameters and isotropic temperature factors are given in Table I.

Structural Results

The bond lengths and bond angles of the MO_4 tetrahedra in $Sr_2(MO_4)Cl$ [M = V, Cr] are given in Table II, in comparison with corresponding data for Ca^{2+} spodiosites. Their site symmetry is approximately D_{2d} with a compression along the pseudo-S_4 axis, which bisects the O(1′)–M–O(2) and O(1)–M–O(2′) angles 2θ. The remaining four angles deviate from each other by at most 1.5°, indicating small lower symmetry

TABLE I

POSITIONAL PARAMETERS, ISOTROPIC TEMPERATURE FACTORS (Å^2), AND ESTIMATED STANDARD DEVIATIONS FOR $Sr_2(MO_4)Cl$ IN SPACE GROUP *Pbcm* (M = V^V, Cr^V; LEFT AND RIGHT, RESPECTIVELY)

	x	y	z	B	x	y	z	B
Sr(1)	0.6249(2)	0.25	0	0.48	0.6228(2)	0.25	0	0.68
Sr(2)	0.1360(1)	0.4663(1)	0.25	0.45	0.1350(2)	0.4653(2)	0.25	0.66
M	0.1278(2)	0.25	0	0.27	0.1246(2)	0.25	0	0.49
O(1)	−0.0300(7)	0.2257(6)	0.1187(4)	0.55	−0.0344(7)	0.2306(7)	0.1183(5)	0.74
O(2)	0.2858(8)	0.4260(6)	0.0291(4)	0.63	0.2836(8)	0.4232(7)	0.0318(5)	0.79
Cl	0.4910(4)	0.1910(4)	0.25	1.50	0.4814(5)	0.1761(5)	0.25	1.60

components. Though V^{5+} and Cr^{5+} have only slightly differing ionic radii—in accord with average V–O and Cr–O spacings of $\approx 1.71_5$ and $\approx 1.69_5$ Å (Table II), respectively—the tetragonal compression is significantly larger for the Cr(V) compared to the V(V) compounds. While the deviation of the tetrahedral angle 2θ from $109.5°$ is $6.5°$ to 7° in the latter cases, it is 9° to 10° for the Cr(V) spodiosites, which may be due to a Jahn–Teller distortion component (see below). Also the tetragonal compression seems to be larger for the Ca^{2+} than for the Sr^{2+} spodiosites by about 10%.

Inspecting the thermal parameters in Table II, it is striking that those of the constituting ions in Sr_2CrO_4Cl are much larger than those in Sr_2VO_4Cl, which may be taken as an indication for a dynamics in the former compound induced by chromium. We will come back to this phenomenon below. Low-temperature structure analyses are in progress to follow this presumable dynamics in dependence on temperature. It is interesting to note that an analogous enhancement of the thermal parameters is observed, going from Ca_2MO_4Cl (M = P, V) to Ca_2CrO_4Cl (*9*, *10*).

Figure 1 sketches the spodiosite structure. From the projection into the *bc*-plane one can deduce that the pseudo-S_4 polyhedron axes lie in this plane, with angles of 36° and 54° with respect to the *b*- and *c*-axis, respectively (for all compounds in Table II).

EPR Data

Mn(V)-Doped Spodiosites

A single-crystal $Sr_2(VO_4)Cl$ (Mn^V doped) with the approximate dimensions 1.0 × 0.5 × 0.2 mm^3 was selected for the EPR analysis. Nicely resolved spectra are observed already at 298 K, which are characteristic for the presence of two magnetically

TABLE II

M–O BOND LENGTH (Å) AND O–M–O BOND ANGLES (°) OF MO_4 TETRAHEDRA IN SPODIOSITE COMPOUNDS $A^{II}(M^VO_4)Cl$

A^{II}, M^V	M–O(1) [2×]	M–O(2) [2×]	O(1)–M–O(1′)	O(1′)–M–O(2) [2×]	O(2)–M–O(2′)	O(1)–M–O(2) [2×]
Ca, P (*9*)	1.550(2)	1.532(2)	107.3(2)	107.3(1)	107.8(2)	113.6(1)
Ca, V (*10*)	1.711(2)	1.703(1)	107.0(1)	105.9(1)	105.6(1)	116.4(1)
Ca, As (*10*)	1.690(1)	1.679(1)	107.2(1)	105.3(1)	105.5(1)	117.1(1)
Ca, Cr (*9*)	1.710(4)	1.689(4)	105.3(3)	104.8(2)	104.4(3)	119.2(2)
Sr, V	1.726(5)	1.715(5)	106.2(2)	106.9(2)	105.5(2)	115.9(2)
Sr, Cr	1.699(5)	1.687(5)	105.4(2)	105.4(2)	104.9(3)	118.3(2)

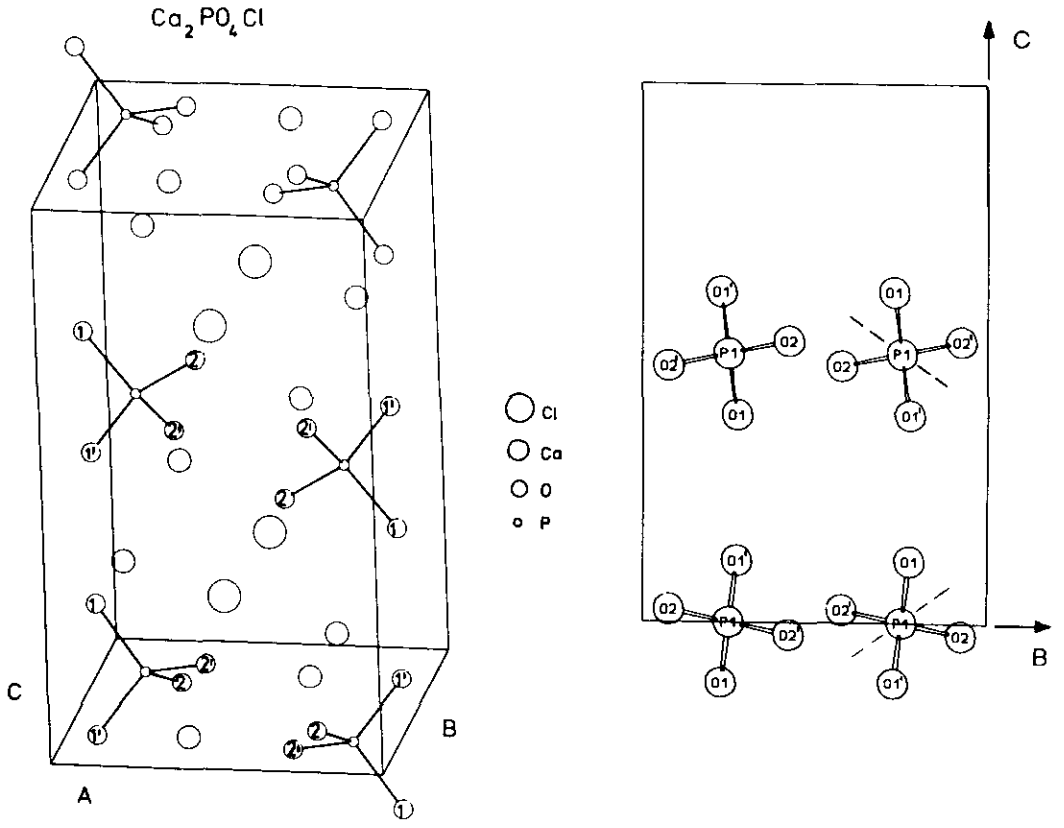

FIG. 1. The orthorhombic unit cell of $Ca_2(PO_4)_4Cl$ (left) and the projection of the four tetrahedra in the cell into the (100) plane (right). The directions of the pseudo-S_4 axes are indicated.

inequivalent MnO_4^{3-} centers. It is immediately evident from the angular dependencies of the fine-structure **D** tensor—for theoretical details, see (*5*)—that the D_z, D_y, and D_x components closely follow the (approximate) D_{2d} symmetry of the tetrahedra (Fig. 2). While D_z ($= 0.32\ cm^{-1}$) is oriented parallel to the pseudo-S_4 axes of the two differently oriented MnO_4^{3-} polyhedra, D_x ($-0.14\ cm^{-1}$) follows the crystallographic a-direction. D_y ($-0.18\ cm^{-1}$) is located in the (100) plane and has, as D_x, the orientation of one of the pseudo-C_2 axes of the MnO_4^{3-} polyhedron. The same angular dependence is characteristic for Mn(V)-doped $Ca_2(MO_4)Cl$ with $M = V^V$, As^V, while for Mn^V in $Ca_2(PO_4)Cl$, D_z and D_y are rotated by $\approx 10°$. We have interpreted this result by assuming that the molecular S_4 axes now have angles of 45° with b and c (*5*), i.e., that the MnO_4^{3-} tetrahedra in the phosphate matrix undergo a rotation around the a-axis. The presumable reason are packing forces, which arise due to the considerably larger ionic radius of Mn(V) compared to P(V) (*5*, *11*).

In Table III zero field splitting parameters D and E of Mn(V)-doped spodiosites $A_2^{II}(MO_4)Cl$ are collected. The expressions, which connect the usually used D and E values and the fine structure components D_i ($i = x, y, z$) are given by

$$2D = |2D_z - (D_x + D_y)|; \quad 2E = |D_x - D_y| \qquad (D_x + D_y + D_z = 0). \quad (1)$$

The D-values are $0.46_5 \pm 0.02$ at 298 K—getting larger with decreasing temperature. At the first glance in contradiction with these data, is the observation that the (pseudotetragonal) symmetry splittings of the d–d

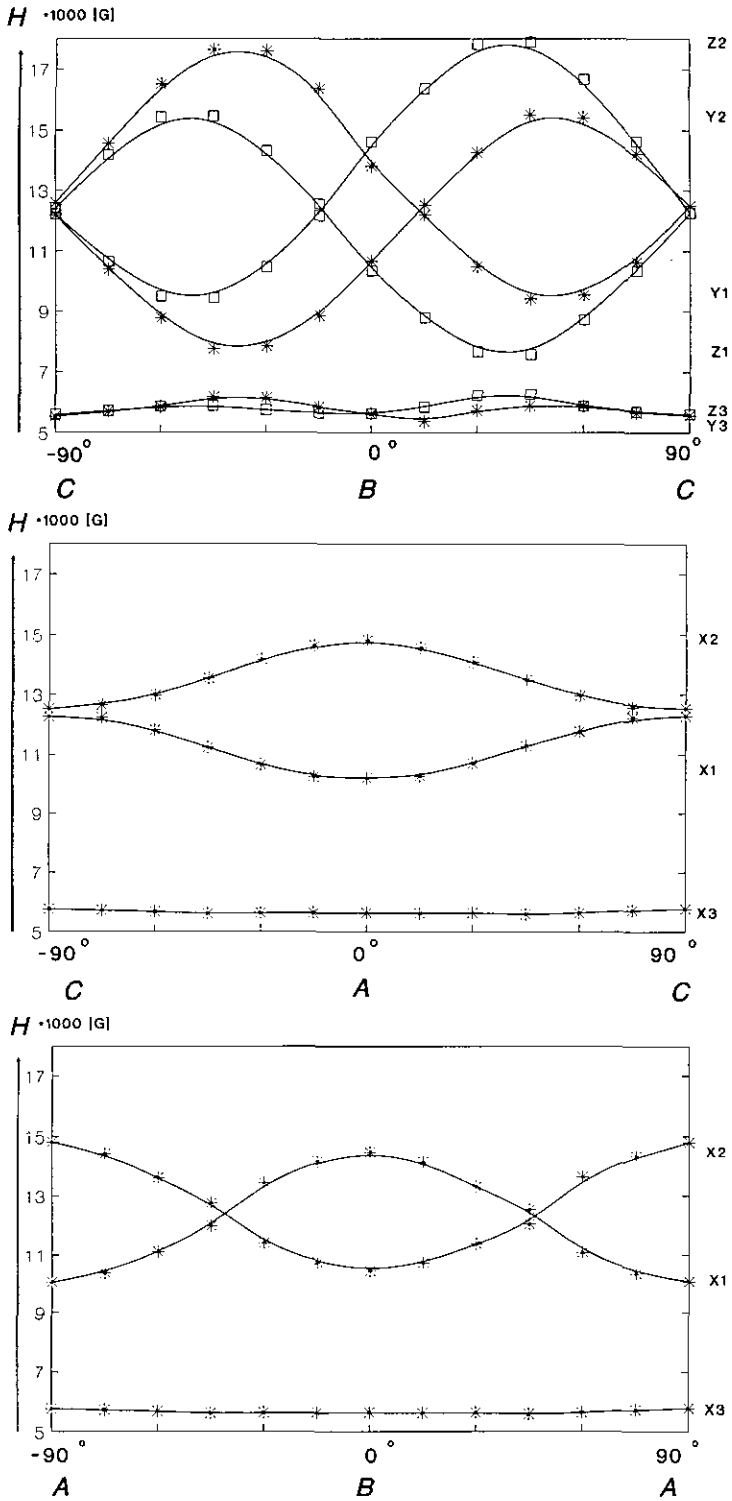

FIG. 2. Angular dependence of the **D** tensor components (298 K) for Mn(V)-doped $Sr_2(VO_4)Cl$ in the (100), (010), and (001) planes. The two differently oriented polyhedra are marked in the (100) plane. The x_i, y_i, and z_i denote the $\Delta M_s = 1$ ($i = 1, 2$) and $\Delta M_s = 2$ ($i = 3$) transitions.

TABLE III

ZERO-FIELD SPLITTING PARAMETERS D, E (cm^{-1}) FOR Mn(V) IN SPODIOSITE-TYPE COMPOUNDS $A_2(MO_4)Cl$ (X- AND Q-BAND POWDER DATA; g = 1.96 ±0.01)

A^{II}, M^{V}	T (K)	D	E	Band
Ca, P	298	0.44_3	0.06_2	Q
	130	0.48_7	0.06_3	Q
Ca, As	298	0.47_0	0.05_3	Q
Ca, V	298	0.45_7	0.03_7	Q
	4	0.50_1	0.04_3	X
Sr, V[a]	298	0.48_4	0.02_2	Q

[a] For this compound (X-band values) there are printing errors in Ref. (*5*).

transitions are about 20% smaller in the Sr^{2+} spodiosite compared to the Ca^{2+} compounds (*5*, *11*), indicating smaller polyhedron distortions than in the former cases. Though the zero field splitting directly reflects these splittings, it is also inversely proportional to the square of the ligand field parameter Δ [see Eq. (2), with ξ being the effective spin–orbit coupling parameter and δE the splitting of the lowest energy $^3A_2 \rightarrow {}^3T_2$ d–d band due to the D_{2d} distortion], however,

$$D \simeq \xi^2 \delta E / \Delta^2. \qquad (2)$$

In spite of the undoubtly more distinct local distortions of the MnO_4^{3-} polyhedra in the Ca spodiosites, the D-value of the Sr compound is slightly larger than those for the former compounds. This is because Δ is reduced for Mn^{5+}-doped Sr_2VO_4Cl by about 7%, which induces an increase of D according to Eq. (2). We have estimated from the d–d transition energies in the ligand field spectrum (*5*) that the 2θ angle bisected by the pseudo-S_4 axis is by about 2° smaller for the MnO_4^{3-} polyhedron in the Sr^{2+} compared to the Ca^{2+} compounds. Indeed these angles differ by 0.5° to 1.0° for the Ca, V–Sr, V and Ca, Cr–Sr, Cr spodiosites, respectively (Table II). We conclude that the spectroscopic properties of Mn^{5+} nicely reflect the geometry of the host MO_4^{3-} tetrahedra in the investigated spodiosites. As will be demonstrated in the next section, this is true only when a closed-shell host cation with a size similar to that of Mn(V) is chosen. In the case of Mn^{5+} there is no influence of the electronic structure on the geometry [orbitally non-degenerate $^3A_2$ (e^2) ground state].

Cr(V)-Doped Spodiosites

We have used the computer program CAMMAG (*7*) to calculate the d–d transitions as well as the g-values and their orientation with respect to the molecular CrO_4^{3-} geometry in the various host spodiosite-type compounds (Table IV). Input data are the geometries of the MO_4^{3-} host sites from structure determinations (Table II) and reasonable AOM parameters, which are derived from the ligand field spectra (*1*, *3*, *4*). e_σ and e_π are AOM parameters (*8*), which describe the σ- and π-antibonding properties of the d-orbitals in the respective polyhedron geometries due to the overlap with the symmetry-adapted ligand orbitals. E_{ds} takes the interaction of the A_1 (d_z^2) ground state with the excited A_1 state resulting from the central ion 4s orbital into account. It was assumed to be of the magnitude ≃1500 cm^{-1}, corresponding to about 10% of e_σ, which seems to be a reasonable value at least for octahedral complexes (*12*). e_σ and e_π were adjusted to the experimental band positions with the assumption $e_\sigma \simeq 4\, e_\pi$ (Table IV). The corresponding ligand field parameter,

$$\Delta = 4/9(3e_\sigma - 4e_\pi), \qquad (3)$$

is ≃12.500 cm^{-1}, nicely reflecting the Δ values of Mn^{5+} in the same host lattices (*5*, *11*).

Surprisingly, it was not possible to obtain a good fit to the experimental results (Table IV). The deviation of the MO_4 polyhedron geometries from the D_{2d} symmetry is so small that, in particular, the observed large orthorhombic splitting of the $^2A_1 \rightarrow {}^2E$ transition (D_{2d}) cannot be reproduced by the

TABLE IV

Cr^{5+}-DOPED SPODIOSITES $A^{II}(MO_4)Cl$: OBSERVED AND CALCULATED [BY CAMMAG] *d–d* TRANSITION ENERGIES,[a] *g*-VALUES, AND ORIENTATIONS OF THE *g*-VALUES[b]

A^{II}, M^V	Exp.[c]	Ca, P[e] calc.	Ca, V[e] calc.	Ca(Sr), Cr[e] calc.	Calc.[f]
$^2A_1 \rightarrow {}^2B_1$	—	0.9	1.4_5	$1.5(1.4_5)$	2.0_5
$^2A_1 \rightarrow {}^2E$	10.7(10.5)	11.9_5	11.5	10.8(11.0)	10.5
	12.1(12.0)	12.1	11.7	10.9(11.1)	12.2
$^2A_1 \rightarrow {}^2B_2$	17.2(16.7)	14.7_5	16.2	$17.2_5(16.9)$	17.2
g_x	1.94_9[d](1.94_5)	1.94_3	1.94_0	1.93_9	—
g_y	1.95_1[d](1.95_0)	1.94_6	1.94_5	1.94_2	—
g_z	$1.99_2(1.99_2)$	2.00_2	2.00_2	2.00_1	—
g_{av}	$1.96_4(1.96_2)$	1.96_4	1.96_2	1.96_1	—
g_x	90°	90°	90°	90°	—
g_y	±36°	$\pm 35.5°$	±35°	±35°(±34°)	—
g_z	±54°	$\pm 54.5°$	±55°	±55°(±56°)	—

Note. Input energy parameters are: e_σ = 14,000 cm^{-1}; e_π = 3500 cm^{-1}; e_{ds} = 1.500 cm^{-1}. Effective LS coupling parameter ξ = 115 cm^{-1}.

[a] Labeling in D_{2d} symmetry, energies in 10^{-3} cm^{-1}.

[b] Angles with respect to the *c*-axis (g_z is always located in the (100) plane).

[c] Values for Cr^{5+}-doped $Ca_2(MO_4)Cl$ (M = P, As, V) and (in parentheses) $Sr_2(VO_4)Cl$.

[d] Values for M = P; in the case of M = V: 1.94_7 and 1.95_3.

[e] Using the structural data of Table II.

[f] Model calculation for an orthorhombic D_2 symmetry with O–M^{5+}–O angles: 118.4° (2×); 107.5° (2×); 102.9° (2×); *g*-values are not listed, because the static CAMMAG calculations cannot reproduce the dynamics of the experimental *g* tensor.

calculation (Fig. 3). Also the $g_\parallel$ value deviates significantly from the one expected for a d_z^2 ground state:

$$g_\parallel = g_0 \quad g_\perp = g_0 - 6u_\perp \qquad [u_\perp = \xi/E(^2A_1 \rightarrow {}^2E)]. \tag{4}$$

We think that vibronic coupling effects of the Jahn–Teller type are responsible for these discrepancies and will discuss this phenomenon first with respect to the *g* tensor and subsequently in respect to the large orthorhombic splitting of the excited $^2T_2$ state (T_d).

(*a*) *g-Tensor.* The linear vibronic coupling constant, which determines the Jahn–Teller splitting of the π-antibonding ^2E ground state, is expected to be considerably smaller than the one of a σ-antibonding state of the same symmetry (Cu^{2+} in octahedral coordination for example), because it is less strongly coupled to the ligand environment (*12*). This implies, that the higher order interaction terms can be assumed to be very small with respect to the energy of the Jahn–Teller active tetrahedral ε mode. In such a case the vibronic coupling leads to a situation, where the electronic ground state doublet has to be replaced by a vibronic quartet (*13*, *14*) with a strong delocalization of the d_z^2 electron toward $d_{x^2-y^2}$, the electronic part of the vibronic Born–Oppenheimer product function being:

$$\psi_g = \alpha d_{z^2} \pm \alpha' d_{x^2-y^2}. \tag{5}$$

A delocalization of the described nature induces the following *g*-tensor components:

$$g_\parallel = g_0 - 4u_\parallel(1 - q)$$
$$g_\perp = g_0 - 4u_\perp(1 + 1/2q) \tag{6}$$
$$\{u_{\parallel(\perp)} = \xi/E[^2A_1 \rightarrow {}^2B_2(^2E)]\}.$$

q is the vibronic reduction factor introduced by Ham (*15*, *13*) and varies between 1 and 1/2. The former value corresponds to the

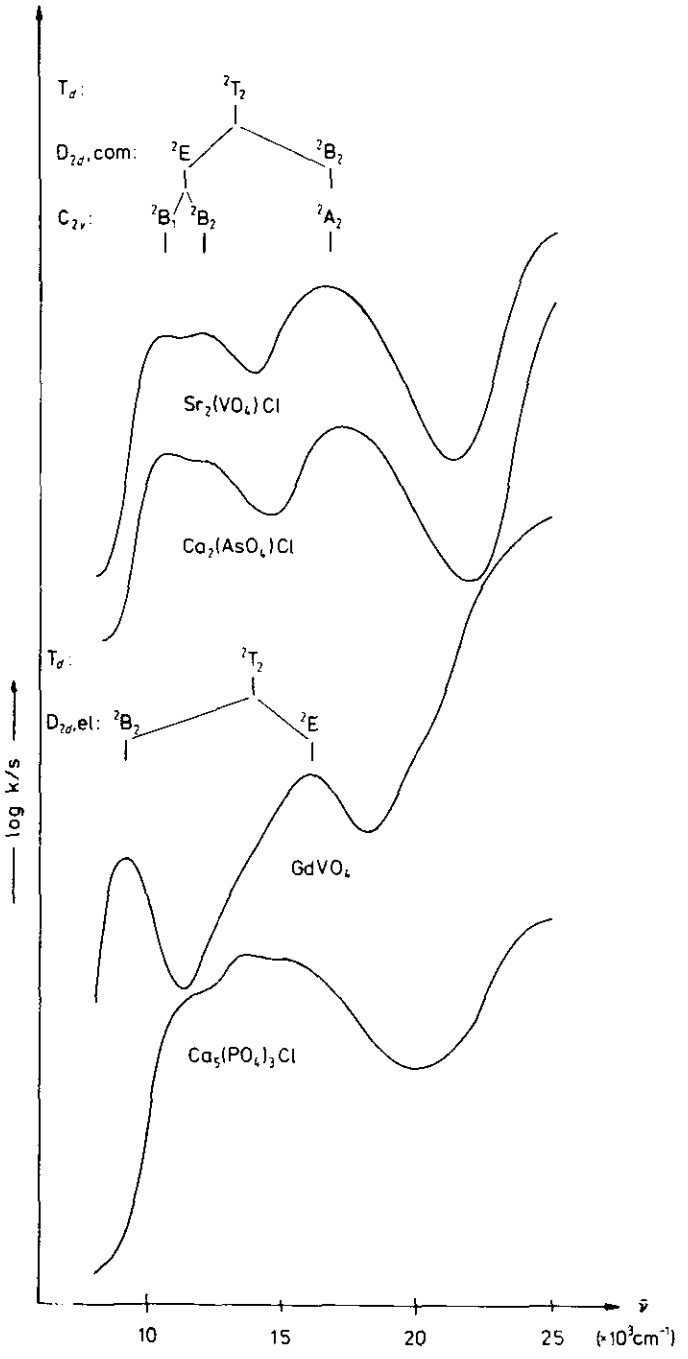

FIG. 3. Ligand field spectra of Cr^{5+}-doped compounds with band assignments. Structural data are given in the text.

static limit of a d_{z^2} ground state (see Eq. (4)), while $q = 1/2$ correlates with $\alpha = 1/2\sqrt{3}$ and $\alpha' = 1/2$ in wavefunction (5) and maximum electronic delocalization.

In order to reproduce the experimental g-values—neglecting the small orthorhombic component (Table II)—and in particular the considerable deviation of $g_\parallel$ from g_0, ξ and

q have to be chosen as $\simeq 115\ cm^{-1}$ and $\simeq 0.6$, respectively. As mentioned before the CAMMAG program does not account for vibronic effects of this kind. Inspecting the CrO_4^{3-} polyhedra, we apparently face an intermediate situation, characterised by the host site strain on the one hand, which tends to localise the system into a d_{z^2} ground state, and a vibronic Jahn–Teller coupling which is partly dynamic, with a distinct electron delocalisation. This delocalization is such, that it stabilises geometries, which are tetragonally elongated along one of the two C_2 axes of the CrO_4^{2-} tetrahedra with pseudo-D_{2d} symmetry, and hence a B_1 ($d_{z^2-x^2}$ or $d_{z^2-y^2}$) ground state. It can be shown indeed by a simple AOM treatment that a B_1 ground state is energetically more stabilized that the alternative A_1 ground state, if the deviation $\delta(2\theta)$ from the tetrahedral angle exceeds $\simeq 5°$ (*17*). From the approximate analytical expression for the reduction factor q (*13*),

$$q = 1/2\{1 + \exp\cdot[-1.974(E_{JT}/h\omega)^{0.761}]\}, \quad (7)$$

and using the reported energy of the ε mode for the CrO_4^{3-} polyhedron ($\simeq 270\ cm^{-1}$) (*16*) one obtains for the energy parameter $E_{JT} \simeq 200\ cm^{-1}$. From this value we can estimate the linear vibronic coupling constant A_1 (*12*),

$$2E_{JT} = A_{1\rho}, \quad (8)$$

where the radial distortion parameter ρ (D_{2d} symmetry) is given by

$$\rho = R|\delta(2\theta)|. \quad (9)$$

ρ is easily calculated from the structural data in Table II (R: M–O spacing), yielding 0.28 Å (angle of compression 119°, $R = 1.69_5$ Å). The derived A_1 value of $\simeq 1500\ cm^{-1}\ Å^{-1}$ is even smaller than expected (see (*17*) for further discussion).

The calculated ground state splitting of $\simeq 2000\ cm^{-1}$ (Table IV, best fit value in last column—see next section) results from the three following contributions: A lowering of d_{z^2} by $\simeq 550\ cm^{-1}$ with an additional contribution due to the 3 d_{z^2} – 4s interaction of $\simeq 400\ cm^{-1}$ and a destabilization of $d_{x^2-y^2}$ by $\simeq 1100\ cm^{-1}$. The energy contribution of 550 cm^{-1} corresponds to 2 E_{JT} (*12*), yielding a Jahn–Teller energy parameter, which is in fair agreement with the value estimated from Eq. (7). The major part of the ground state splitting (≈70%) is apparently due to the host site strain of the spodiosite lattice (D_{2d} compressed, with a small orthorhombic component), as can be deduced by inspecting the distortions of the MO_4 polyhedra in the vanadium and arsenium compounds in comparison to those in the chromium spodiosites (Table II). V^{5+} and As^{5+} have ionic radii nearly equal to the one of Cr^{5+}, but spherically symmetric ground states. The Jahn–Teller contribution to the distortion will be distinctly larger than 30%, if the underlying additional distortion component, which is dynamically averaged, is also taken into account.

Delocalisation effects of the kind described above are even more evident inspecting the g and hyperfine values of Cr^{5+} in host lattices Li_3MO_4 (M = P, V, As) (*18*), imposing only very small non-random strains on the CrO_4^{3-} polyhedra. Similarly, the structural data of Cr^{5+} apatites in comparison to the chromium-free compounds also indicate an additional Jahn–Teller contribution to the strain-induced distortion of the CrO_4^{3-} polyhedra. A more rigorous treatment of the vibronic $E \otimes \varepsilon$ coupling for tetrahedrally coordinated d^1 cations in the presence of nonrandom strains will be given elsewhere (*17*).

(*b*) *Optical spectra.* The rather large orthorhombic component in the splitting of the excited tetrahedral T_2 state cannot be reproduced by CAMMAG calculations on the basis of the available structural data (Table IV). We have performed model calculations for a compressed tetrahedron with a variable lower symmetry D_2 component, however, and have found that a good agreement with the experimental band positions is achieved with the AOM parameters of Table IV and O–M–O bond angles of

118.4° (2×), 107.5° (2×), and 102.9° (2×). This very significant lower symmetry component is interpreted as originating from the dynamic admixture of $d_{x^2-y^2}$ into the d_{z^2} ground state (with mixing coefficients $1 > \alpha > \sqrt{3}/2$ in Eq. (5)). While this component is dynamically averaged in the g-values, see Section (a), it is nicely resolved in the ligand field spectra, because the time scale is shorter by several orders of magnitude than the one for EPR transitions on the one hand, and the orthorhombic splitting of the excited $^2T_2$ state is much more distinct on the other hand, because it is in past σ-antibonding in contrast to the only π-antibonding character of the ^2E ground state.

It seemed interesting to us to compare the presented results with those of Cr^{5+} in tetragonally elongated host tetrahedra, which are found in host compounds $A^{III}VO_4$ [A^{III} = Nd, Y, Er], for example. The VO_4 polyhedra of D_{2d} symmetry have 2θ angles between 100.2° and 100.9° (*19*). The ligand field spectrum of the Cr^{5+}-doped compounds exhibit two bands at 9300 and 16 500 cm^{-1} (Fig. 3) and the g-values are indicative of a B_1 ground state. The band positions can be nicely reproduced with AOM parameters e_σ = 14 700 cm^{-1}, e_π = 3700 cm^{-1}, which are very similar to those of Table IV, and a 2θ angle of 98°. Again—as in the case of compressed tetrahedra—a static Jahn–Teller contribution enhances the extent of the site distortion. A dynamic component is not present, as expected, and the observed g-values ($g_\parallel$ = 1.90_3 and $g_\perp$ = 1.98_8) are those calculated with ξ = 115 cm^{-1} on the basis of a purely static distortion:

$$g_\parallel = g_0 - 8u_\parallel \quad g_\perp = g_0 - 2u_\perp \qquad (10)$$
$$[u_\parallel = \xi/E(^2B_1 \rightarrow {}^2B_2);\ u_\perp = E(^2B_1 \rightarrow {}^2E)].$$

The ground state splitting is estimated to be 3650 cm^{-1}, if the e_{ds} value of Table IV is used.

Figure 3 compares the ligand field spectra of compressed CrO_4^{3-} tetrahedra in spodiosite-type compounds with the case just discussed and with Cr^{5+} in the only slightly distorted tetrahedra of a chloride apatite. The proper assignments are indicated. Due to the energetic position of the color-determining minimum, the spodiosites are blue, the apatite compound is green, and Cr^{3+}-doped $GdVO_4$ is yellowish green.

Similar vibronic effects as for Cr^{5+} show up in the g and hyperfine values as well as in the optical spectra of V^{4+} in a tetrahedral oxo-coordination (*20*). We have extended these measurements to various other VO_4^{4-}-doped oxidic compounds and will report the results separately (*21*).

Conclusions

We have noted before that the fine-structure components D_i (i = x, y, z) of MnO_4^{3-} polyhedra isomorphously doped into Ca_2PO_4Cl do not follow the symmetry of the PO_4^{3-} host tetrahedra. We have interpreted the EPR results by proposing that the pseudo-S_4 axis is rotated by 10°, and have traced back this behavior to packing effects in the lattice due to the different ionic radii of P^{5+} and Mn^{5+} (*5*, *11*).

Surprisingly Cr^{5+}, though of comparable size with Mn^{5+}, does not show this geometrical effect in the same host compound (*2*). We think that the dynamics induced by the vibronic instability of the ^2E ground state ($E \otimes \varepsilon$ coupling) gives the CrO_4^{3-} polyhedra enough geometric flexibility to adapt to the host compound without orientational changes. We have assumed in this discussion that in the case of Mn^{5+} the fine-structure tensor and in the case of Cr^{5+} the g-tensor exactly reflect the geometry of the doped MnO_4^{3-} and CrO_4^{3-} polyhedra.

The assumption of strong dynamical electronic delocalization effects in the case of compressed CrO_4^{3-} tetrahedra in spodiosite-type compounds is additionally supported by two results:

1. The thermal parameters of the constituting atoms of Sr_2CrO_4Cl are much larger than those of the corresponding vanadium spodiosite (Table I). An analogous situation is found for the thermal parameters of Ca_2

CrO_4Cl (*9*) compared with those of Ca_2PO_4Cl (*9*) and Ca_2VO_4Cl (*10*). This anomalous behavior possibly indicates dynamical atomic movements in the chromium compounds due to vibronic coupling.

2. The Jahn–Teller active ε mode has been observed for tetrahedrally oxo-coordinated chromates for the oxidation states +6, +5, and +4 (*16*). While for the totally symmetric α_1 mode a steady decrease from 846 to 834 to 806 cm^{-1} is reported with decreasing oxidation state, a striking discontinuity is observed for the ε vibration. It appears at 348 and 353 cm^{-1} for CrO_4^{2-} and CrO_4^{4-}, respectively, but at 260 cm^{-1} in the case of CrO_4^{3-}, which indicates soft-mode behavior of this particular vibration—as would be expected for a dynamical $E \otimes \varepsilon$ vibronic interaction.

Acknowledgments

We appreciate the funding by the German–Israeli Foundation for Scientific Research & Development and also owe thanks to Dr. M. Atanasov, Sofia, for valuable discussions and U. Kesper for experimental assistance.

References

1. L. Disipio, L. Oleari, and P. Day, *J. Chem. Soc. Faraday Trans.* **68,** 776 (1972).
2. E. Banks, M. Greenblatt, and B. R. McGarvey, *J. Chem. Phys.* **47,** 3772 (1967).
3. D. Reinen, C. Albrecht, and U. Kaschuba, *Z. Anorg. Allg. Chem.* **584,** 71 (1990).
4. R. Borromei, L. Oleari, and P. Day, *J. Chem. Soc. Faraday Trans.* **73,** 135 (1977); **77,** 1563 (1981).
5. H. Lachwa and D. Reinen, *Inorg. Chem.* **28,** 1044 (1989).
6. M. Herren, H. U. Güdel, C. Albrecht, and D. Reinen, *Chem. Phys. Lett.* **183,** 98 (1991); M. Herren, T. Reidener, H. U. Güdel, C. Albrecht, U. Kaschuba, and D. Reinen, *J. Luminescence* **53,** 452 (1992).
7. D. A. Cruse, J. E. Davies, J. H. Harding, M. Gerloch, D. J. Mackey, R. F. McMeeking, CAMMAG, a FORTRAN PROGRAM.
8. C. K. Jorgensen, R. Pappalardo, and H.-H. Schmidtke, *J. Chem. Phys.* **39,** 1442 (1963); C. E. Schäffer, and C. K. Jorgensen, *Mol. Phys.* **9,** 401 (1965).
9. M. Greenblatt, E. Banks, and B. Post, *Acta Crystallogr. Sect. B* **23,** 166 (1967); **25,** 2170 (1969).
10. E. Banks, M. Greenblatt, and B. Post, *Inorg. Chem.* **9,** 2259 (1970).
11. D. Reinen, H. Lachwa, and H. Allmann, *Z. Anorg. Allg. Chem.* **542,** 71 (1986).
12. M. Atanasov, and D. Reinen, *Magn. Res. Rev.* **15,** 167 (1991) and cited references.
13. I. B. Bersuker, "The Jahn–Teller Effect and Vibronic Interactions in Modern Chemistry," Plenum Press, New York–London (1984). [Series Editor: J. P. Fackler, Jr.]
14. R. E. Coffman, *J. Chem. Phys.* **48,** 609 (1968).
15. F. S. Ham, *Phys. Rev.* **138,** 1727 (1965).
16. F. Gonzales-Vilchez, and W. P. Griffith, *J. Chem. Soc. Dalton Trans.*, 1416 (1972) and cited references.
17. M. Atanasov, D. Reinen, in preparation.
18. M. Greenblatt, and J. H. Pifer, *J. Chem. Phys.* **70,** 116 (1979).
19. H. Fuess, A. Kallel, *J. Solid State Chem.* **5,** 11 (1972); G. Schmidt, B. Deppisch, V. Gramlich, and C. Scheringer, *Acta Crystallogr. B* **29,** 141 (1973).
20. S. Di Gregorio, M. Greenblatt, J. H. Pifer, and M. D. Sturge, *J. Chem. Phys.* **76,** 2931 (1982).
21. U. Kesper, W. Rańw, M. Atanasov, M. A. Hitchman, and D. Reinen submitted for publication.